Chinese Chemical Letters 34 (2023) 107426

Contents lists available at ScienceDirect

Chinese Chemical Letters

journal homepage: www.elsevier.com/locate/cclet

Lithium storage properties of $Ti_3C_2T_x$ (T_x = F, Cl, Br) MXenes

Pengcheng Liu[a], Peng Xiao[a], Ming Lu[b], Hui Wang[c], Na Jin[a], Zifeng Lin[a,d,*]

[a] College of Materials Science and Engineering, Sichuan University, Chengdu 610065, China
[b] The Joint Laboratory of MXene Materials, Key Laboratory of Functional Materials Physics and Chemistry of the Ministry of Education, Jilin Normal University, Changchun 130103, China
[c] Institute for Advanced Study, Chengdu University, Chengdu 610106, China
[d] Engineering Research Center of Alternative Energy Materials and Devices, Ministry of Education, Chengdu 610065, China

ARTICLE INFO

Article history:
Received 23 March 2022
Revised 6 April 2022
Accepted 7 April 2022
Available online 12 April 2022

Keywords:
MXene
Molten salt synthesis
Halogen termination
Li^+ storage
Electrochemistry

ABSTRACT

In this work, $Ti_3C_2T_x$ MXene with -F, -Cl and -Br surface terminations are synthesized and the effect of these halogen terminations on the lithium storage properties is investigated. A maximum Li^+ storage capacity of 189 mAh/g is achieved with $Ti_3C_2Br_x$ MXene much higher than $Ti_3C_2Cl_x$ and $Ti_3C_2F_x$ with 138 mAh/g and 123 mAh/g, respectively. Density functional theory (DFT) calculation shows that the adsorption formation energy of halogen atoms on Ti atoms follows the trend of Ti-F > Ti-Cl > Ti-Br, leading to the same trend in the content of terminations on corresponding MXenes. In addition, inevitable exposure of MXene to oxygen causes competition between halogen and oxygen. Theoretical results show $Ti_3C_2Br_x$ MXene has the highest Ti to O ratio and the lowest Ti to Br ratio, the high lithium affinity of O explains the maximum Li-ion storage capacity with $Ti_3C_2Br_x$ MXene. This work shed light on the opportunity for achieving improved lithium storage properties of MXene electrodes by regulating the surface chemistry.

Two-dimensional (2D) transition metal carbides and/or nitrides (MXenes) have shown broad application prospects in the fields of energy storage [1–4], sensing [5], electromagnetic shielding [6], and catalysts [7] due to their rich surface chemistry, excellent electronic transmission capacity [8], and unique hydrophilicity [9]. MXenes are derived from the top-down selective chemical etching of A layer atoms of bulk MAX phase precursors with a formula of $M_{n+1}AX_n$ (n = 1, 2, 3, *etc.*), where M stands for an early transition metal element (Ti, Nb, V, Mo, *etc.*), A is an element from IIIA and IVA (Al, Si, *etc.*), and X represents carbon and/or nitrogen. Correspondingly, the general formula of MXene is $M_{n+1}X_nT_x$ (n = 1, 2 or 3), with T_x representing the surface terminations. One of the advantages of MXenes compared to other 2D materials (*e.g.*, graphene) is that the surface chemistry of MXenes materials can be tuned and engineered. The surface terminations play an indispensable role in affecting the properties of MXene materials, such as hydrophilicity, electronic and optical properties. The surface terminations of MXenes can be controlled by selecting the etching agent during the preparation and substitution and elimination reactions post the synthesis. For instance, HF aqueous solution [10] or LiF + HCl mixtures [11] etching routes have been the common methods used to synthesize MXenes, achieving MXenes with -F, -O and -OH mixed terminations. $Ti_3C_2T_x$ MXene with -OH and -O termination was prepared through an alkali-assisted hydrothermal method [12]. A recent important method of a general Lewis acidic molten salt etching route was proposed to synthesize -Cl and -Br riched MXenes without -F and -OH, and the surface chemistry of molten salt derived MXenes was further posted synthetically modified to a large group of elements, including -NH, -S, -Se, -Te [13–15].

By tuning the surface functional groups, the properties of MXenes can be engineered for various applications, in particular of Li-ion storage [13,16–18]. Many theoretical and experimental studies have shown the influence of surface terminations on lithium-ion storage, in which the oxygen terminated MXenes show the highest lithium-ion storage capacity and high Li^+ mobilities [19–21]. Meanwhile, the stability of different functional groups terminated MXenes was also predicted theoretically with the following trend of $Ti_3C_2O_2$ > $Ti_3C_2F_2$ > $Ti_3C_2(OH)_2$ > $Ti_3C_2H_2$ > Ti_3C_2, making it possible to further regulate the types and contents of surface functional groups in pursuing better active materials for Li-ion storage [22].

Previous experimental and theoretical works that study the role of surface terminations in electrochemical energy storage are

* Corresponding author at: College of Materials Science and Engineering, Sichuan University, Chengdu 610065, China.
E-mail address: linzifeng@scu.edu.cn (Z. Lin).

https://doi.org/10.1016/j.cclet.2022.04.024
1001-8417/

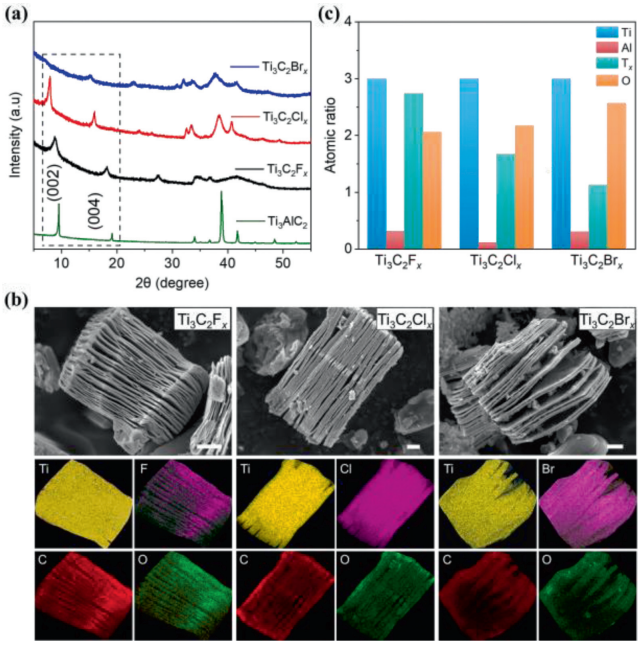

Fig. 1. (a) XRD patterns of pristine Ti_3AlC_2 MAX phase and halogenated $Ti_3C_2T_x$ Mxenes. (b) SEM images and corresponding EDS mapping of $Ti_3C_2T_x$ MXenes with -F, -Cl, and -Br surface terminations, scale bar is 1 μm. (c) Comparison of the elemental composition of halogenated $Ti_3C_2T_x$ MXenes.

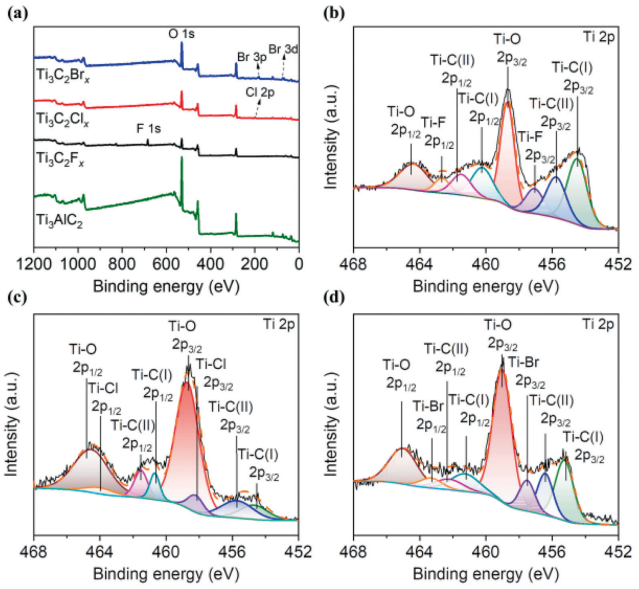

Fig. 2. XPS analysis of the Ti_3AlC_2 precursor and halogenated MXenes. (a) The overview of XPS spectrum and Ti 2p analysis of MXenes surface terminations with (b) -F, (c) -Cl and (d) -Br.

mainly related to -O, -OH and -F. Since the surface chemistry is limited by the conventional preparation process involving the HF-containing etching solutions [19,23]. However, there is scarce systematic research on how halogen terminations affect lithium-ion storage. Herein, we synthesized -F, -Cl, -Br terminated $Ti_3C_2T_x$ MXenes and investigated the influence of halogen surface terminations on the electrochemical performance of lithium-ion storage.

Conventional HF-based etching and molten salt etching routes are used to obtain -F terminated MXene and -Br/-Cl terminated MXenes, respectively [10,13]. The XRD patterns of pristine Ti_3AlC_2 MAX phase and halogenated $Ti_3C_2T_x$ are shown in Fig. 1a. The diffraction peaks of Ti_3AlC_2 are significantly weakened after the etching process. The 2θ of (002) diffraction peak of $Ti_3C_2F_x$ is 8.82° and $Ti_3C_2Cl_x$ is 7.86°, which corresponds to c values of 20.04 Å and 22.48 Å, respectively. The c value of $Ti_3C_2Br_x$ is 23.16 Å based on the (004) peak at $2\theta = 15.29°$. These results are in good agreement with the previous report [13]. SEM images and corresponding EDS mapping of halogenated $Ti_3C_2T_x$ MXenes are shown in Fig. 1b. The halogenated MXenes show a typical accordion morphology with opened laminae and semi-quantitative EDS analyses show the uniform distribution of Ti, C, O, and halogen elements on the MXene particles. The atomic ratio of Ti:Br ≈ 3:1.1 means that the halogen atoms are partially occupied at the surface terminal sites (Table S1 in Supporting information). Fig. 1c compares the elemental compositions of halogen MXenes. The aluminum contents of the prepared MXenes samples are reduced significantly, indicating that the Al layer is selectively removed. In addition, the F_x content is much higher than Br_x and Cl_x contents, while the oxygen contents show the opposite trend.

The composition and chemical state of halogenated MXenes are further investigated by X-ray photoelectron spectroscopy (XPS) analysis. Fig. 2a shows the overview of the XPS spectrum of Ti_3AlC_2 MAX phase and prepared halogenated $Ti_3C_2T_x$. For Ti_3AlC_2, the signals of Ti 2p, C1 s, and Al 2p are observed at 458, 285 and 74 eV, respectively. The peak position of Al 2p at 74.8 eV of $Ti_3C_2Cl_x$ corresponds to the Al-O bond, which indicates an oxide layer on the aluminum surface (Fig. S1 in Supporting information) [24]. The Ti-Al bond signal at 73.4 eV and the Al-Al signal at 71.5 eV are absent in the XPS spectrum of halogenated MXenes, suggesting the removal of aluminum (Fig. S1). Furthermore, the peak of Al-O detected from MXenes prepared by molten salt can be explained by the hydrolysis of aluminum halide or the presence of Al_2O_3 from the precursor [24]. Meanwhile, the F, Cl and Br signals are detected in the spectra of $Ti_3C_2F_x$, $Ti_3C_2Cl_x$ and $Ti_3C_2Br_x$ MXene, respectively, confirming the presence of halogen surface groups.

Figs. 2b–d show the signal of Ti 2p spectra of halogenated MXenes. The existence of Ti-F ($2p_{3/2}$), Ti-Cl ($2p_{3/2}$), and Ti-Br ($2p_{3/2}$) chemical bonds at the peak positions of 457.0, 458.2 and 457.5 eV are originated from -F, -Cl, and -Br surface functional groups [14,24–27]. Furthermore, the F 1s, Cl 2p and Br 3d (Fig. S2 in Supporting information) signal prove the existence of the Ti-F, Ti-Cl and Ti-Br bonds, the presence of oxygen surface termination and the Ti-C bond is also verified by the fittings of O 1s (Fig. S3 in Supporting information) and C 1s spectra (Fig. S4 in Supporting information). More detailed information of XPS analysis is shown in Supporting information (Figs. S1–S4 and Tables S2–S4 in Supporting information). Hence, we confirmed that the MXene surface in this work is predominantly terminated with halogens and oxygens.

To shed light on the origin of terminations on $Ti_3C_2T_x$ MXenes, it is instructive to identify the most energetically favorable chemisorption sites. As reported in the previous works [13,22], the top of Ti_2 (Ti_1 and Ti_2 represent the outer layer Ti and the central layer Ti, respectively) is the most stable chemisorption site. According to DFT calculations, the adsorption formation energy of -F, -Cl, -Br and -O is −5.339, −3.638, −2.781 and −4.943 eV, respectively. The more negative value is, the more preferable and stable the termination of adsorption will be. As such, the stability of various halogenated $Ti_3C_2T_x$ follows the order: $Ti_3C_2F_2$ > $Ti_3C_2Cl_2$ > $Ti_3C_2Br_2$. Furthermore, the charge redistributions were calculated to reveal the bonding strength between each termination and host MXenes. As shown in Fig. S5 (Supporting information), electronic cloud density shows the degree of charge transfer connected to the bonding strength, further indicating the stability of MXenes with different surface terminations: $Ti_3C_2O_2$ ≈ $Ti_3C_2F_2$ > $Ti_3C_2Cl_2$ > $Ti_3C_2Br_2$.

Bader charge analysis also provides a methodology to quantitatively estimate the extent of charge transfer. Table S5 (Support-

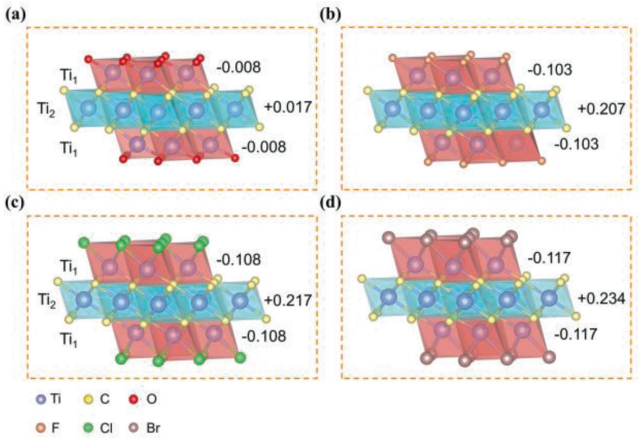

Fig. 3. (a-d) Bader charge analysis of octahedra in terminated $Ti_3C_2T_2$ (T = O, Br, Cl, F) MXenes. The rea and blue octahedra represent Ti_1-C_3T_3 and Ti_2-C_6 octahedrons, respectively.

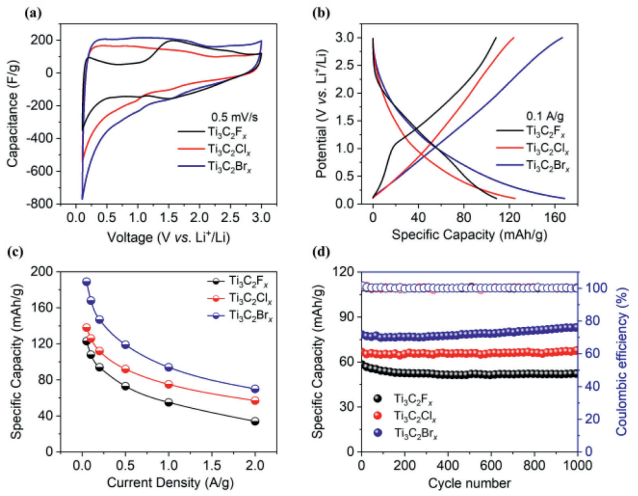

Fig. 4. Electrochemical performance of halogenated MXenes electrodes. (a) Cyclic voltammetry curves at 0.5 mV/s. (b) Galvanostatic charge-discharge profiles at a current of 0.1 A/g. (c) Capacities under different current densities. (d) Long cycling performance at a current density of 1 A/g for l000 cycles.

ing information) lists the charge transfer of each atom on $Ti_3C_2T_2$. Generally, the surface termination has a more significant impact on the surface Ti_1 than central Ti_2. As for surface Ti_1, the Bader charge increase from 37.02% to 66.61%, and C and central Ti_2 increased by 6.33% and 0.7%, taking $Ti_3C_2Br_2$ as a case, elucidating the impact degree of surface termination. Further analysis demonstrates that $Ti_3C_2T_2$ owes different stability when taking octahedra as building blocks. As presented in Fig. 3, two types of octahedra are marked as red and blue, which shows the ability to accommodate electrons. Except for $Ti_3C_2O_2$, nearly neutral, the Ti_1-C_3T_3 octahedron of other $Ti_3C_2T_2$ tends to devote electrons to central Ti_2-C_6, giving rise to the heterolytic octahedra carrying a significant amount of positive charges. The classical crystal-chemical theory argues that charged octahedra should lead to Coulomb repulsion and structure destabilization [28]. Therefore, based on the ability to accept electrons of the octahedron in $Ti_3C_2T_2$, the stability follows the order: $Ti_3C_2O_2$ > $Ti_3C_2F_2$ > $Ti_3C_2Cl_2$ > $Ti_3C_2Br_2$, which is in good agreement with the calculations above.

The MXenes prepared previously have also verified different chemisorption abilities. Since O is an unavoidable factor during the synthesis, the surface terminations of $Ti_3C_2T_x$ would be distributed according to the competitiveness of each element. The chemisorption capability somehow determines the termination content, resulting in increasing O content in halogenated $Ti_3C_2T_x$ follows as $Ti_3C_2Br_x$ > $Ti_3C_2Cl_x$ > $Ti_3C_2F_x$, which has also been confirmed from EDS. The previous simulation has suggested that the Li-ion storage capability of MXenes is strongly bonded with the surface terminations, and the -O terminated $Ti_3C_2T_x$ gives the highest capacity [19].

To investigate the lithium-ion storage performance of halogenated MXenes, MXenes electrodes are prepared by mixing with carbon-containing conducting additive/binder (see experimental section in Supporting information). To compare the electrochemical behavior of different halogen terminated MXenes, stabilized cyclic voltammetry curves are shown in Fig. 4a. The $Ti_3C_2Br_x$ electrode gives a maximum specific capacitance up to 152 mAh/g at a scan rate of 0.5 mV/s in the potential range from 0.1 V to 3 V *versus* Li^+/Li. Whereas $Ti_3C_2Cl_x$ and $Ti_3C_2F_x$ exhibit lower specific capacities of 106 mAh/g and 96 mAh/g. The electrochemical signal of $Ti_3C_2F_x$ MXene obtained by HF etching is significantly different from the signals obtained by the molten salt derived MXenes electrodes. Specifically, the $Ti_3C_2F_x$ electrode has a reduction peak at 1.49 V and an oxidation peak at 1.56 V. In contrast, no obvious redox peaks are observed for $Ti_3C_2Cl_x$ and $Ti_3C_2Br_x$ electrodes, which is similar to the intercalation-type pseudocapacitive behavior reported elsewhere [29]. Cyclic voltammetry profiles of halogenated MXenes at various scan rates (from 0.2 mV/s to 10 mV/s) are shown in Fig. S6 (Supporting information). Furthermore, the non-diffusion capacities are estimated by using the Trasatti plot method. As presented in Fig. S7 (Supporting information), $Ti_3C_2Br_x$ exhibits the highest total capacities and non-diffusion capacity, and the non-diffusion capacity accounts for more than 50% of the total capacities, which indicates the high-rate properties of the $Ti_3C_2Br_x$ MXene electrodes. While $Ti_3C_2F_x$ electrode delivers much less non-diffusion charge contribution. Fig. 4b presents the galvanostatic charge-discharge curves at a current density of 0.1 A/g after cycling, the reversible specific capacities of $Ti_3C_2F_x$, $Ti_3C_2Cl_x$ and $Ti_3C_2Br_x$ are 108, 126 and 168 mAh/g, respectively. Fig. 4c shows the rate performance of the halogenated MXenes at current densities from 0.05 A/g to 2 A/g. The $Ti_3C_2F_x$, $Ti_3C_2Cl_x$ and $Ti_3C_2Br_x$ deliver maximum capacities of 123, 138, and 189 mAh/g at a current density of 0.05 A/g, respectively. At a current density of 2 A/g, $Ti_3C_2Br_x$ maintains a capacity of 70 mAh/g, demonstrating its good rate properties. Furthermore, the long cycle performance at a current density of 1 A/g is shown in Fig. 4d. The three MXene electrodes exhibit excellent cycling performance with no capacity attenuation after 1000 cycles. The galvanostatic charge-discharge curves of halogenated MXenes at different specific currents are tested (Fig. S8 in Supporting information) after cycling tests at a current density of 1 A/g. The above results prove that the types of surface terminations significantly impact the lithium storage performance of MXenes electrodes in nonaqueous electrolytes, and the larger *c*-value of $Ti_3C_2Br_x$ MXene may also enhance the electrochemical properties [30,31]. The electrochemical performances of halogenated $Ti_3C_2T_x$ are the following order of $Ti_3C_2Br_x$ > $Ti_3C_2Cl_x$ > $Ti_3C_2F_x$.

In summary, we have synthesized three halogenated MXenes including $Ti_3C_2Br_x$, $Ti_3C_2Cl_x$, and $Ti_3C_2F_x$. It is found that halogen surface terminations have important effects on Li-ion storage capacity. The maximum specific capacities of $Ti_3C_2Br_x$, $Ti_3C_2Cl_x$ and $Ti_3C_2F_x$ are 189, 138 and 123 mAh/g, respectively, matching well with the trend of O contents on corresponding MXenes. It is believed that halogen elements with the lowest binding energies with MXene will lead to high O surface groups when exposed to an oxygen environment, thus, achieving more Li-ion storage capacity thanks to the high lithium affinity of O surface groups.

Declaration of competing interest

The authors declare that they have no known competing financial interests or personal relationships that could have appeared to influence the work reported in this paper.

Acknowledgments

This study was funded by the National Natural Science Foundation of China (No. 52072252), Sichuan Science and Technology Program (No. 2020ZDZX0005), the Fundamental Research Funds for the Central Universities (No. YJ201886), and Center of "11" Future Science Jilin 11 Technology Co., Ltd.

Supplementary materials

Supplementary material associated with this article can be found, in the online version, at doi:10.1016/j.cclet.2022.04.024.

References

[1] C.F. Zhang, L. McKeon, M.P. Kremer, et al., Nat. Commun. 10 (2019) 1795.
[2] B. Guan, X. Sun, Y. Zhang, et al., Chin. Chem. Lett. 32 (2021) 2249–2253.
[3] J. Luo, X. Lu, E. Matios, et al., Nano Lett. 20 (2020) 7700–7708.
[4] J. Luo, J. Zheng, J. Nai, et al., Adv. Funct. Mater. 29 (2019) 1808107.
[5] W. Yuan, X. Qu, Y. Lu, et al., Chin. Chem. Lett. 32 (2021) 2021–2026.
[6] Y. Yao, J. Zhao, X. Yang, C. Chai, Chin. Chem. Lett. 32 (2021) 620–634.
[7] T. Xu, J. Wang, Y. Cong, et al., Chin. Chem. Lett. 31 (2020) 1022–1025.
[8] M.K. Han, C.E. Shuck, R. Rakhmanov, et al., ACS Nano 14 (2020) 5008–5016.
[9] Y. Gogotsi, B. Anasori, ACS Nano 13 (2019) 8491–8494.
[10] M. Naguib, M. Kurtoglu, V. Presser, et al., Adv. Mater. 23 (2011) 4248–4253.
[11] M. Ghidiu, M.R. Lukatskaya, M.Q. Zhao, Y. Gogotsi, M.W. Barsoum, Nature 516 (2014) 78–81.
[12] T. Li, L. Yao, Q. Liu, et al., Angew. Chem. Int. Ed. 57 (2018) 6115–6119.
[13] M. Li, X.L. Li, G.F. Qin, et al., ACS Nano 15 (2021) 1077–1085.
[14] V. Kamysbayev, A.S. Filatov, H.C. Hu, et al., Science 369 (2020) 979–983.
[15] Y.B. Li, H. Shao, Z.F. Lin, et al., Nat. Mater. 19 (2020) 894–899.
[16] H.Y. Dong, P. Xiao, N. Jin, et al., ChemElectroChem 8 (2021) 957–962.
[17] F.Y. Kong, X.D. He, Q.Q. Liu, et al., Electrochim. Acta 265 (2018) 140–150.
[18] Z. Bao, C. Lu, X. Cao, et al., Chin. Chem. Lett. 32 (2021) 2648–2658.
[19] Y. Xie, M. Naguib, V.N. Mochalin, et al., J. Am. Chem. Soc. 136 (2014) 6385–6394.
[20] Q. Tang, Z. Zhou, P. Shen, J. Am. Chem. Soc. 134 (2012) 16909–16916.
[21] M. Lu, H.J. Li, W.J. Han, et al., J. Energy Chem. 31 (2019) 148–153.
[22] T. Hu, Z.J. Li, M.M. Hu, et al., J. Phys. Chem. C 121 (2017) 19254–19261.
[23] X. Wang, X. Shen, Y. Gao, et al., J. Am. Chem. Soc. 137 (2015) 2715–2721.
[24] M. Li, J. Lu, K. Luo, et al., J. Am. Chem. Soc. 141 (2019) 4730–4737.
[25] J. Halim, K.M. Cook, M. Naguib, et al., Appl. Surf. Sci. 362 (2016) 406–417.
[26] I. Persson, L.A. Naslund, J. Halim, et al., 2D Mater. (2018) 015002.
[27] V. Natu, M. Benchakar, C. Canaff, et al., Matter 4 (2021) 1224–1251.
[28] A.R.J. West, Solid State Chemistry and Its Applications, 2 ed., John Wiley & Sons Ltd., New York, 2014.
[29] W.Y. Chen, X.F. Jiang, S.N. Lai, D. Peroulis, L. Stanciu, Nat. Commun. 11 (2020) 1302.
[30] Z.Y. Gu, J.Z. Guo, J.M. Cao, et al., Adv. Mater. (2022) 2110108.
[31] M.Y. Wang, X.X. Zhao, J.Z. Guo, et al., Green Energy Environ. 7 (2022) 763–771.